

Antibody Multispecificity Mediated by Conformational Diversity

Leo C. James,¹ Pietro Roversi,² Dan S. Tawfik^{3*}

A single antibody was shown to adopt different binding-site conformations and thereby bind unrelated antigens. Analysis by both x-ray crystallography and pre-steady-state kinetics revealed an equilibrium between different preexisting isomers, one of which possessed a promiscuous, low-affinity binding site for aromatic ligands, including the immunizing hapten. A subsequent induced-fit isomerization led to high-affinity complexes with a deep and narrow binding site. A protein antigen identified by repertoire selection made use of an unrelated antibody isomer with a wide, shallow binding site. Conformational diversity, whereby one sequence adopts multiple structures and multiple functions, can increase the effective size of the antibody repertoire but may also lead to autoimmunity and allergy.

Since the identification of antibodies at the end of the 19th century, scientists have sought to explain how a limited repertoire of antibodies can bind and thereby protect against an almost infinite diversity of invading antigens. The discovery of clonal selection revealed that the combinatorial arrangement of a rather small number of different antibody gene segments has the potential to generate a highly diverse repertoire of antibodies. However, the number of antibodies in the primary response is finite, whereas antigen space is effectively limitless. A possible explanation is that each antibody is capable of binding more than one antigen. Such a scenario was envisaged in the 1940s. Pauling proposed that specific binding sites were selected out of an ensemble of preexisting antibody conformations (1). Indeed, antibodies have been shown to cross-react with multiple antigens ever since they were discovered (2–6). The first immunologists also realized that cross-reactivity, in addition to expanding the antibody repertoire, could result in the immune system turning against the organism it is meant to defend, or in Ehrlich's chilling words, *horror autotoxicus* (3). Cross-reactivity is now known to play a central role in autoimmunity and allergy (7, 8). The ability to distinguish between invading antigens and self-proteins can be bypassed when antibodies raised against pathogenic antigens pro-

miscuously bind self-antigens or innocuous environmental molecules (9, 10).

Antibodies are renowned for their exquisite specificity, so how can they be both promiscuous and specific? Structures of antibody fragments that have been cocrystallized with different steroid molecules demonstrate that cross-reactivity can be accomplished through shared ligand chemistry or molecular mimicry (11, 12). The D1.3 antibody to lysozyme binds both lysozyme and an anti-idiotypic antibody through the rearrangement of several side chains (13). An antibody to the HIV-1 protein p24 also binds several other peptides that fit into the same binding site (6). These studies demonstrate that a single antibody-binding site can accommodate different, if related, ligands. However, Pauling had proposed an equilibrium between different preexisting structural isomers (pre-equilibrium), each of which provides a different binding site and binding specificity. Many antibodies exhibit different crystal structures in their free and bound states (14, 15). In the absence of solution kinetics, however, structural differences between free and complexed antibodies are generally ascribed to an induced-fit mechanism [in which the ligand binds the free structure and induces a conformational change leading to the complexed structure (14)] rather than to pre-equilibrium. Although there is no structural evidence for pre-equilibrium, there are kinetic studies that unambiguously demonstrate its existence. Pecht (16), followed by Foote and Milstein, revealed the operation of both pre-equilibrium and induced fit in antibodies; the latter also postulated that conformational diversity might have fundamental implications for the immune response (17). To date, however,

there has been no structural evidence for equilibrium between preexisting antibody isomers or that different isomers of the same antibody can bind different antigens.

Here we describe our studies of antibody SPE7, a monoclonal immunoglobulin E (IgE) raised against a 2,4-dinitrophenyl (DNP) hapten (18, 19). SPE7 exhibits high affinity [a dissociation constant (K_d) of 20 nM] and specificity toward DNP; its affinity for close analogs of DNP, such as 2-nitrophenol (NP) and 2-nitro-4-iodophenol, is negligible ($K_d > 100 \mu\text{M}$) (20). However, screening has revealed that SPE7 also binds several unrelated compounds with a broad range of affinities (5), such as alizarin red (Az, $K_d = 40 \text{ nM}$) and furazolidone (Fur, $K_d = 1.2 \mu\text{M}$). We have also used repertoire selections to identify a protein antigen of SPE7 (Trx-Shear3). Data obtained by x-ray crystallography and pre-steady-state kinetics show that SPE7 adopted at least two different preexisting conformations that were independent of antigen, each conferring a different antigen-binding function.

Crystal structures of SPE7 reveal its conformational diversity. In the absence of antigen, the Fv heterodimer of SPE7 crystallized in two different conformations (Ab^1 and Ab^2), which have entirely unrelated L3 and H3 loop configurations (Table 1 and Fig. 1). Four crystal structures of SPE7 complexed with four different antigens were also determined. In three of these complexes, with the haptens DNP-Ser, Az, or Fur, a third antibody conformation was observed, termed Ab^3 . Finally, when complexed to a recombinant protein antigen (Trx-Shear3), SPE7 adopted a fourth conformation, Ab^4 . The six structures therefore indicate that SPE7 can adopt at least four different binding-site configurations (Fig. 1). Both free antibody-binding sites formed solvent-exposed channels, albeit in perpendicular orientations. In Ab^1 , this channel was flatter and more regular, whereas in the alternative isomer (Ab^2) it was funnel-shaped and terminated in a deep pocket. In the hapten-bound antibody (Ab^3), neither of these channels was present, but a deep pocket reminiscent of Ab^2 was seen. The protein-bound antibody isomer (Ab^4) had a relatively flat binding site, with a truncated version of the channel as observed in Ab^1 .

The four different antibody conformations involved large backbone alterations in the L3 and H3 loops (Fig. 2D). There are two distinct L3 conformations, centered around tryptophan residue 93L (Trp93L). In the free isomer Ab^1 and the Trx-Shear3-bound isomer Ab^4 , Trp93L formed the base of a shallow cleft. In the free isomer Ab^2 and the hapten isomer Ab^3 , Trp93L is flipped up to create a deep pocket.

¹Centre for Protein Engineering, Medical Research Council Centre, Hills Road, Cambridge CB2 2HQ, UK.

²Global Phasing Ltd., Castle Hill, Cambridge, UK. ³Department of Biological Chemistry, The Weizmann Institute of Science, Rehovot 76 100, Israel.

*To whom correspondence should be addressed. E-mail: tawfik@weizmann.ac.il

This movement is accompanied by a displacement of the L3 main chain by up to 2 Å and by the rotation of several side chains. Root mean square deviations (rmsds) of the superposed free structures (Ab¹ and Ab²) showed that Trp93L and residue Asn96L differ in position by more than 5 Å (measured between the NE1 and Cδ atoms, respectively) (Fig. 2D). The H3 loop displayed even greater variation; the different loop configurations start to diverge at Met99H and do not realign until Tyr109H. The C-αs from the free isomers deviate on average by 4.5 Å, with the most substantial difference at Tyr105H (6.7 Å). In addition to adopting unrelated main-chain conformations, each isomer displayed different side-chain rotamers. Residues Trp33H, Arg50H, and Tyr101H, which stack together and form the top end of the cleft in free isomer Ab¹, are all rotated by 90° in the hapten-complexed isomer (Ab³). In the alternative free isomer Ab², however, Tyr101H stacks against Trp100H and the main chain at H107, folding the loop into the interior of the antibody.

How do the free isomers relate to the complexed structures? The surface, H3, and L3 loops of Ab¹ are entirely unrelated to the hapten-complexed structure (Ab³). Ab², however, has much in common with Ab³: an identical L3 conformation (including Trp93L) and a similar narrow pocket. Furthermore, it is unlikely that from an initial encounter complex with Ab¹, the bound ligand could have induced the final complexed conformation Ab³. All the aromatic ligands bind SPE7 by stacking in between Trp93L and Tyr105H (Fig. 2). Stacking of the ligand against Trp93L in its Ab¹ conformation and a subsequent change leading to Ab³ would end up with the ligand on the “wrong” side of the tryptophan, stacked against the L3 main chain rather than against Tyr105H. The structures therefore suggest that hapten binding occurred through the preexisting isomer Ab².

Pre-steady-state binding kinetics. To determine the dynamics of the binding process, we examined the pre-steady-state kinetics of complex formation between SPE7 and DNP-Ser, as well as between SPE7 and the hapten cross-reactants. The kinetics confirmed the existence of an equilibrium in solution between two preexisting isomers, only one of which bound the haptens. Pre-steady-state binding kinetics were analyzed by monitoring changes in SPE7's intrinsic fluorescence upon rapid mixing with ligand (21). A single-step bimolecular association of antibody with ligand would have resulted in a single exponential decay in fluorescence. However, the fluorescence quenching observed upon binding of SPE7 to either the immunizing hapten (DNP) or the cross-reacting haptens (Az and Fur) showed a complex pattern that can only be described by three exponentials, each decaying at a different

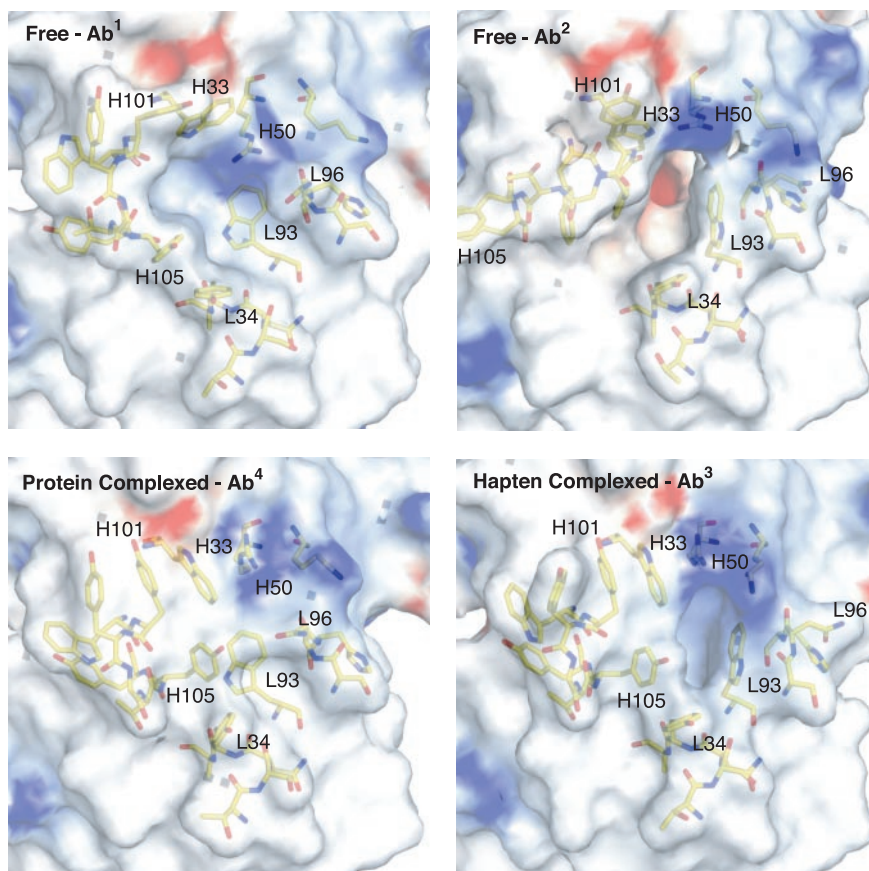


Fig. 1. The four different isomers of IgE antibody SPE7. A close-up view of the binding site is shown as a semitransparent surface, colored according to electrostatic potential (blue for positive, red for negative). The figure was prepared with GRASP (39, 40) and AESOP (41). The Ab³ and Ab⁴ models are presented without ligand.

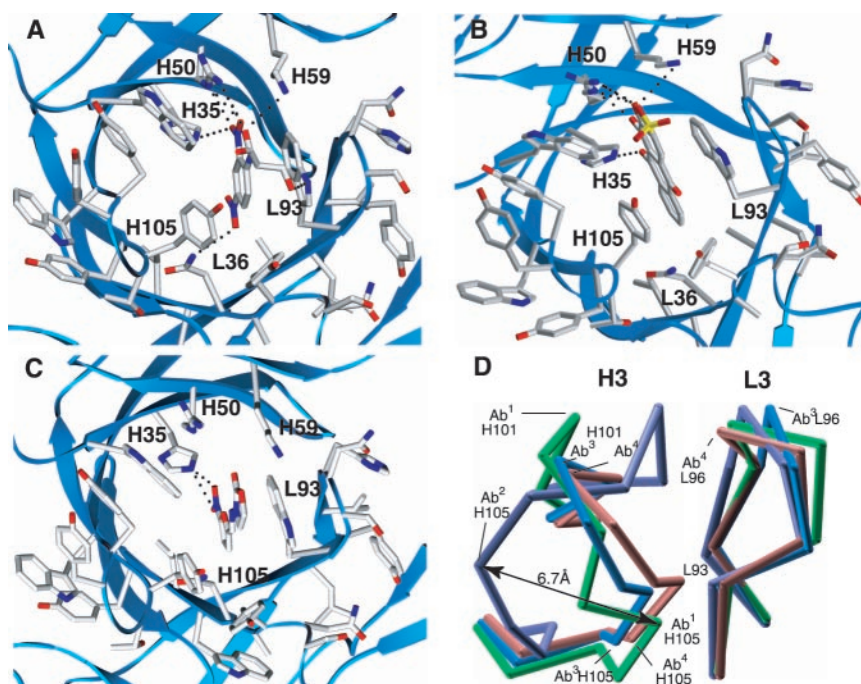


Fig. 2. Details of SPE7's binding site and main-chain superposition of isomers. (A to C) Hapten-bound SPE7 with (A) DNP-Ser, (B) Az, and (C) Fur. Putative hydrogen bonds are indicated by dotted spheres between acceptor and donor atoms. (D) Main-chain configurations of free isomers Ab¹ (green) and Ab² (purple), hapten-bound isomer Ab³ (blue), and Trx-Shear3-bound isomer Ab⁴ (ochre). All figures were prepared with SETOR (41).

RESEARCH ARTICLES

rate. The fast phase occurred over ~ 10 ms and the intermediate phase over ~ 100 ms, whereas the slow phase persisted for several seconds (Fig. 3). The individual phases were separated and fitted to a single exponential to give an observed rate constant ($k_{\text{obs}} = 1/\tau$, where τ is the reciprocal relaxation time). This experiment was repeated at different ligand concentrations.

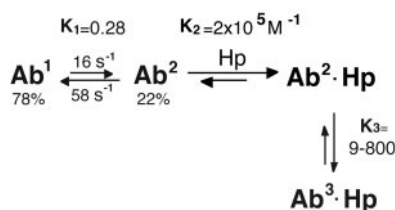
The observed rate of the fast phase exhibited a linear dependency on hapten concentration (Fig. 3, upper inset) that is consistent with a simple bimolecular association of antibody with ligand. For all three haptens tested, a second-order association rate (k_2) typical of haptens binding a preexisting cavity was observed [$k_2 = (3.4 \text{ to } 9.5) \times 10^6 \text{ M}^{-1} \text{ s}^{-1}$] (17). The dissociation rates (k_{-2}) are also very similar ($k_{-2} = 66 \text{ to } 126 \text{ s}^{-1}$). The

resulting affinity constants ($K_2 = k_2/k_{-2}$) for these antibody-hapten complexes ($\text{Ab}^2 \cdot \text{Hp}$) are therefore relatively low [$(1 \text{ to } 3) \times 10^5 \text{ M}^{-1}$]. The rate of the intermediate phase decreased with ligand concentration (Fig. 3, lower inset). This pattern is consistent with an equilibrium between two preexisting antibody conformers, only one of which binds the ligand (16, 17). As expected, the fit of this phase gave essentially the same kinetic parameters regardless of the type of hapten: the forward rate for isomerization (k_1) is $16 \pm 2 \text{ s}^{-1}$ and the reverse rate (k_{-1}) is $58 \pm 3 \text{ s}^{-1}$. The data therefore fit a model in which two conformational isomers are in equilibrium at a ratio of about 1:4, the isomerization half-life is ~ 9 ms, and the minor isomer (Ab^2) binds all three haptens with $\sim 20 \mu\text{M}$ affinity (Scheme 1).

We ascribe the slow phase to an induced-fit isomerization of the antibody-ligand encounter complex ($\text{Ab}^2 \cdot \text{Hp}$) to give the final complex ($\text{Ab}^3 \cdot \text{Hp}$). This step is unimolecular and first-order in its kinetics and is kinetically separated from the previous steps. The rate is therefore independent of ligand concentration (as observed), and its kinetic constants cannot be directly determined. However, the binding affinities of the haptens at equilibrium allow us to deduce that the in-

duced-fit isomerization increases the overall affinity by ~ 500 -fold for DNP-Ser, by ~ 800 -fold for Az, and by only 9-fold for Fur.

Correlating structures and kinetics. The simplest model that is consistent with both the crystal structures and the pre-steady-state kinetics describes an equilibrium between two preexisting isomers, only one of which (Ab^2) binds the haptens. We ascribe the predominant free isomer observed structurally (Fig. 1, Ab^1) to the kinetic nonbinding isomer (Scheme 1, Ab^1) and the alternative free isomer (Fig. 1, Ab^2) to the hapten-binding isomer (Scheme 1, Ab^2). There are several observations that support this assignment. First, Ab^1 is the predominant isomer both in solution and in the crystalline state: Ab^1 crystallized under many different conditions, whereas the other isomer (Ab^2) crystallized in only one, high-solvent-exclusion condition. Furthermore, the same kinetic parameters were observed in phosphate-buffered saline and in crystallization buffer (Table 1, buffer A), suggesting that the solution kinetics and crystal structures sampled the same isomeric equilibrium. Second, Ab^2 had Trp93L conformation that is identical to the final hapten-complexed Ab^3 . Stacking of the haptens against Trp93L in the encounter complex ($\text{Ab}^2 \cdot \text{Hp}$, Scheme 1) is consistent with the



Scheme 1.

Table 1. Data collection and structure refinement statistics (37). Numbers in parentheses are for the highest resolution shell. Buffers used were as follows: A, 1 M sodium citrate (pH 6.2); B, 0.1 M Hepes (pH 7.5) and 70% 2-methyl-2,4-pentandiol C, 25% polyethylene glycol 4000 (PEG 4K) 0.1 M sodium acetate, and 0.2 M NH_4SO_4 (pH 5.6); D, 21% PEG 8K,

0.1 M sodium cacodylate, and 0.2 M sodium acetate (pH 5.5); E, 22% PEG 8K, 0.1 M sodium cacodylate, and 0.2 M sodium acetate (pH 5.0); F, 28.5% PEG 4K, 0.1 M magnesium acetate, 0.1 M NH_4SO_4 , and 0.1 M sodium acetate (pH 6.5). I/σ is the ratio of scatter to observations; a.u., asymmetric unit.

	Free* (Ab^1)	Free (Ab^2)	DNP-Ser (Ab^3)	Az (Ab^3)	Fur (Ab^3)	Trx-Shear3 (Ab^4)
Space group	$P2_12_12_1$	$I4$	$P2_12_12_1$	$P2_12_12_1$	$P2_12_12_1$	$P2_12_12_1$
Cell	a = 36.54 b = 70.74 c = 82.12	a = 79.54 b = 79.54 c = 67.70	a = 79.46 b = 79.48 c = 168.91	a = 78.92 b = 78.88 c = 169.04	a = 79.17 b = 79.14 c = 168.91	a = 79.35 b = 79.47 c = 170.77
Copies per a.u.	1	1	4†	4†	4†	2‡
Buffer	A	B	C	D	E	F
Resolution	1.5 Å	2.0 Å	1.8 Å	2.2 Å	2.4 Å	2.7 Å
Unique reflections	34,284	14,044	90,267	52,239	47,809	27,717
R_{merge}	0.0431 (0.238)	0.061 (0.335)	0.070 (0.235)	0.067 (0.325)	0.126 (0.583)	0.086 (0.375)
Redundancy	12.6	4.4	3.0	13.7	6.7	11.0
Percent complete	92.8 (92.8)	99.4 (96.1)	91.8 (91.4)	99.6 (99.4)	99.2 (94.7)	99.2 (95.3)
Average I/σ	6.3 (2.2)	19.2 (5.2)	10.9 (1.8)	9.5 (2.5)	9.9 (3.1)	7.3 (2.6)
Final R_{cryst}^{\S}	0.160	0.21	0.226	0.212	0.258	0.207
Final R_{free}^{\S}	0.182	0.252	0.269	0.243	0.280	0.270
Bond rmsd	0.005	0.005	0.008	0.007	0.013	0.009
Angle rmsd	1.2°	1.3°	1.4°	1.3°	1.5°	1.4°
$\alpha V_{\text{H}}V_{\text{L}}^{\parallel}$	178.2°	173.7°	HL: 174.6° JN: 174.6° KI: 170.7° MO: 167.6°	HL: 173.5° JN: 173.7° KI: 172.5° MO: 170.1°	HL: 174.9° JN: 175.2° KI: 174.5° MO: 170.2°	HL: 174.9° JN: 174.9°
PDB accession codes	1O AQ	1O CW	1O AU	1O AR	1O AY	1O AZ

*The free antibody Ab^1 was also crystallized in buffers C to E and in 1 M lithium chloride (pH 6). The structures crystallized in lithium and buffer C were fully refined and aligned against the citrate structure with an rmsd of <0.1 Å (all atoms). †In these structures, N, I, and O are noncrystallographic symmetry (NCS)-related H chains; J, K, and M are NCS-related L chains. During refinement, tight NCS restraints were used to constrain I to H and O to N in the ranges 1 to 23, 37 to 49, 66 to 94, and 108 to 122, and to constrain J to L and M to K in the ranges 1 to 22, 37 to 48, 61 to 84, and 96 to 101. ‡In this structure, the above ranges were used to apply tight NCS restraints to chains J and N. The two copies of the thioredoxin model in the a.u. (chains A and B) were refined with medium NCS constraints on all residues, B to A. §Final R factors are for all reflections. R factors for the highest resolution bin are as follows: Free Ab^1 : R_{cryst} 0.155; R_{free} 0.175. Free Ab^2 : R_{cryst} 0.177; R_{free} 0.192. DNP-Ser complex: R_{cryst} 0.222; R_{free} 0.258. Az complex: R_{cryst} 0.209; R_{free} 0.271. Fur complex: R_{cryst} 0.248; R_{free} 0.271. Trx-Shear3 complex: R_{cryst} 0.201; R_{free} 0.262. $\parallel \alpha = \arccos[0.5 \cdot (\text{trace } R^{-1})]$, with R being the rotation matrix to rotate the V_{H} chain onto the V_{L} chain; the R matrix was computed using the CCP4 program LSQKAB (38), matching the following stretches of residues by least squares: H1 to H25 \rightarrow L1 to L25; H26 to H42 \rightarrow L27 to L43; H43 to H51 \rightarrow L44 to L50; H52 to H59 \rightarrow L51 to L54; H61 to H102 \rightarrow L55 to L96; H107 to H120 \rightarrow L97 to L110. JN, KI, and MO are the chain definitions for the NCS-related copies as specified above.

large drop in fluorescence that followed formation of this complex (>75% of the total change) (Fig. 3). In contrast, the fluorescence change accompanying the induced-fit isomerization was relatively low (~15% of the overall amplitude), suggesting that this step did not involve major changes in the position of the fluorescing tryptophan. The structures also suggest that isomerization of the encounter complex to the final bound state does not involve movement of Trp93L but rather flipping of H3 into the binding site. This flipping closes the funnel and packs the hapten between Trp93L and Tyr105H and may allow the marked change in affinity associated with this isomerization (9- to 800-fold) without substantially altering antibody fluorescence. However, at this stage we do not have direct

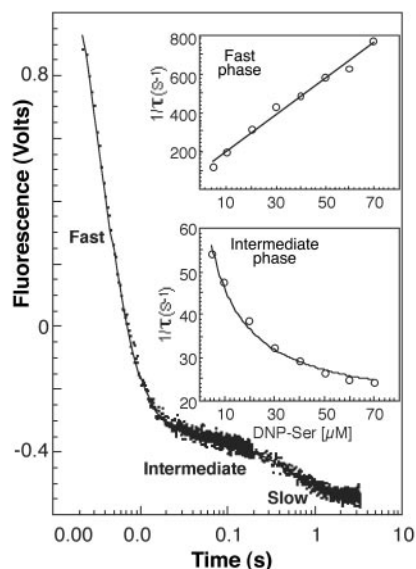


Fig. 3. Pre-steady state fluorescence quenching of SPE7 on addition of DNP-Ser (20 μM) fitted to three exponentials (27). The three phases (fast, intermediate, and slow) roughly separate into time scales of 0.01, 0.1, and 1 s, respectively. Similar experiments were performed at different DNP concentrations ranging from 10 to 70 μM . The three phases were separated and fit independently to a single exponential to give the observed rate constants ($1/\tau = k_{\text{obs}}$). (**Upper inset**) $1/\tau$ from the fast phases plotted against ligand concentration and fit to a standard bimolecular association model: $1/\tau_1 = k_{\text{obs}} = k_{-2} + k_2[L]$, where $[L]$ is the ligand concentration to give $k_2 = (9.5 \pm 0.5) \times 10^6 \text{ M}^{-1} \text{ s}^{-1}$, $k_{-2} = 96 \pm 20 \text{ s}^{-1}$, and an equilibrium constant of $K_2 = k_2/k_{-2} = (1 \pm 0.26) \times 10^5 \text{ M}^{-1}$. (**Lower inset**) $1/\tau$ from the intermediate phases was fit to a pre-equilibrium model (17): $1/\tau_2 = k_{\text{obs}} = k_1 + k_{-1}[K_2/([L] + K_2)]$, where $K_2 = k_2/k_{-2}$, to give $k_1 = 17 \pm 1 \text{ s}^{-1}$, $k_{-1} = 58 \pm 3 \text{ s}^{-1}$ and $K_2 = (1.9 \pm 0.6) \times 10^{-5} \text{ M}$. This value of K_2 is only about twice as high as that obtained by the independent fit of the fast phase [$(1 \pm 0.26) \times 10^5 \text{ M}^{-1}$]. Furthermore, when the former value of K_2 [$(1 \pm 0.26) \times 10^5 \text{ M}^{-1}$] is introduced into the pre-equilibrium model, values within the error range for k_1 and k_{-1} are obtained.

structural evidence for the hapten-induced conformational change. Although the kinetic and structural data indicate two preexisting isomers, they do not exclude the existence of others. Ab^2 could have been in equilibrium with an isomer that already had an H3 conformation, such as the hapten-complexed Ab^3 . Indeed, an H3 conformation related to Ab^3 was seen independently in Ab^4 (Figs. 1 and 2D).

The hapten-SPE7 complexes. The crystal structures of the hapten complexes indicate that the SPE7 binding site adjusted to the specific chemistry of each hapten (Fig. 2, A to C). The differences between the complexed structures are nevertheless subtle and involve less than 2 Å of side-chain movement, except for residue Lys59H, which is more flexible. Binding appeared to be driven primarily by a rather indiscriminate stacking interaction between Trp93L and Tyr105H, the side chains of which move like the jaws of a vise to accommodate the different haptens. The binding specificity and affinity can be explained by the number and nature of the hydrogen bonds each hapten formed with SPE7. DNP-Ser, which had the highest affinity ($K_d = 20 \text{ nM}$), appeared to form the largest number of hydrogen bonds, with residues Glu36L, His35H, and both NE and NH1 groups of Arg50H and Lys59H. Az ($K_d = 40 \text{ nM}$) formed a similar number of hydrogen bonds, whereas Fur, which binds with much lower affinity ($K_d = 1.2 \mu\text{M}$), made only one specific contact. Affinity measurements of close analogs of both DNP and the haptenic cross-reactants also indicate that SPE7's selectivity is mediated by hydrogen bonding. For example, anthraquinone, which is identical to Az except that it lacks the

3,4-hydroxy and 2-sulphate groups that hydrogen-bond to Arg50H and Lys59H (Fig. 2B), exhibited no measurable affinity. We have also found no correlation between the hydrophobicity of various hapten derivatives and their binding affinity (22).

A protein antigen binds a third antibody conformer. To determine whether the conformational diversity of SPE7 enables it to bind completely different antigens, we performed protein library selections to find a protein antigen that would be unrelated to the immunizing hapten (DNP) and the haptenic cross-reactants. The selection system used (FliTrx) displays a library of peptides on the active-site loop of thioredoxin (23). Repertoire selection yielded a family of cyclic peptides, displayed on thioredoxin, that bind SPE7 specifically (Trx-proteins, Fig. 4). Binding was competitively inhibited by both DNP and cross-reactants Az and Fur with inhibitory concentration (IC_{50}) values that reflect their affinities toward SPE7. Linear peptides derived from the loop sequences of the selected Trx-proteins bound SPE7 with barely detectable affinity. Thus, SPE7 appeared to recognize the selected peptide sequences in the context in which they were selected, in a cyclic configuration and as part of the thioredoxin protein. The affinities of the selected Trx-proteins, measured by a competitive enzyme-linked immunosorbent assay with immobilized DNP-asparagine, were $\sim 10 \mu\text{M}$. Such affinities are typical of the FliTrx system, because of the multivalency of its display (23). Although low, these μM -scale affinities are physiologically relevant. IgMs of the primary immune response are active at $> \mu\text{M}$ affinities, largely because they too use multivalency of binding to offset low affinity (24).

We cocrystallized the SPE7 Fv fragment with a recombinant thioredoxin protein that carries one of the selected peptide sequences (Trx-Shear3). In contrast to the deep and narrow hapten-binding sites observed in the hapten complexes (Ab^3), in binding this protein antigen, SPE7 adopted a rather shallow, solvent-exposed binding site reminiscent of protein-binding antibodies (Ab^4 , Fig. 1). The L3 loop conformation was essentially identical to Ab^1 (Fig. 2D), yielding a shallow binding site with Trp93L at the bottom. However, because of a different H3 conformation, the cleft is smaller than in Ab^1 and was attenuated by Tyr105H. Two interaction points were seen between SPE7 and Trx-Shear3 (Fig. 5). First, a loop between residues A104 and A109 of thioredoxin fit into a shallow groove at SPE7's binding-site surface to exclude solvent. The hydroxyl group of Tyr34L was positioned to hydrogen-bond with the NE2 atom of Gln109A and/or the peptide nitrogen of Leu108A, and the peptide nitrogen of Ala107 was positioned to interact with the main-chain oxygen of Tyr101H. The second set of contacts was between the consensus sequence found in the

	A35	40	45
DNP1	I E E	K D G R	T D L H G
DNP2	V E E	K S L W	L Q T E G
DNP3	I E E	P R I L	F G E P I
DNP4	I E E	P G V V	V P G L D
DNP5	I E E	G T D K	D R L H G
DNP6	V E E	R A Y R	V D E T G
Shear1	L E E	L T L Y	Q G I G A
Shear2	V E E	T E R I	V L S N R
Shear3	I E E	S D D R	R Y D L V
Shear4	I E E	R D L R	R G M T E
Shear5	I E E	K V M R	G L G E A
Shear6	V Q E	E Q E R	R R D I G
	I E E	.	R

Fig. 4. The selected Trx-protein ligands. We performed two independent selections, eluting either nonspecifically by shear force (shear) or by specific competition with DNP-Ser (DNP) [(19), section 4]. The consensus sequence is ϕEExxxR , where ϕ is a small hydrophobic group (isoleucine or valine) (41). The numbering corresponds to the residue order in the x-ray model, where chain A is the Trx-protein.

RESEARCH ARTICLES

selected peptide loops (thioredoxin residues A35 to A45) and SPE7's H3 loop. In the Trx-Shear3:antibody structure, residues Trp100H, Tyr101H, and Tyr102H formed a narrow ledge on the antibody surface. The conserved small hydrophobic group at the beginning of the selected peptide (IleA35 in Trx-Shear3) stacked against Tyr102H, fitting into the ledge. The role of the conserved Glu36A is not clear; it packed against the antibody surface but there was no indication of hydrogen-bond interaction. The third consensus residue, Glu37A, was orientated toward thioredoxin, where it anchors the A34-A46 flexible loop against the scaffold, enforcing an α -helix-like twist. The close packing of the entire loop against the antibody surface suggests that the selected peptide is indeed a conformational epitope.

Determining how Ab⁴ relates to the other SPE7 isomers is not straightforward, because the low affinity and intrinsic fluorescence of Trx-Shear3 prevented the measurement of pre-steady-state binding kinetics. However, the structural relationships between the various SPE7 isomers suggest that Ab⁴ had its origins in a third preexisting isomer and that the conformational diversity of SPE7 may well be greater than indicated by the two free structures (Fig. 1, Ab¹ and Ab²). The haptens bound SPE7 with an L3 conformation observed in free isomer Ab², whereas Trx-Shear3 bound with the L3 conformation from Ab¹. However, both the haptens and Trx-Shear3 bound a similar H3 conformation that was not present in either free isomer Ab¹ or Ab². Thus, a third preexisting (free) isomer with an H3 conformation similar to Ab³ and Ab⁴ is a possibility.

Cross-reactivity mediated by a promiscuous antibody isomer. We found two different modes of multispecificity that were both directly linked to the antibody's conformational diversity. The first mode allows

binding of a series of small aromatic ligands, including the immunizing hapten, to a similar binding-site configuration. Although these ligands varied considerably, binding was based on shared ligand chemistry or molecular mimicry of the immunizing hapten with small adaptations of SPE7's binding site. This mode of cross-reactivity was observed in the crystal structures of several antibodies complexed with cross-reactants (6, 11, 12). However, these structures do not reveal the dynamics of the binding process. Here we show that the cross-reactivity of SPE7 was mediated by a promiscuous, low-affinity preexisting isomer (Ab²) that bound DNP and the other small aromatic haptens with low affinity. A subsequent induced-fit isomerization that led to the final hapten-antibody complexes (Ab³) customized hydrogen bonding and stacking interactions. The fast dissociation rate (~ 100 s⁻¹) from the promiscuous transient isomer ensured that stacked ligands that were unable to induce a conformational change and interact via specific hydrogen and electrostatic bonds dissociated immediately. Dissociation of unsuitable ligands may also be linked to the fast relaxation of Ab² to the nonbinding isomer Ab¹ (~ 58 s⁻¹). Thus, the combination of fast relaxation to a nonbinding isomer, on the one hand, and induced-fit isomerization, on the other, provides a "kinetic proof-reading" mechanism that compensated for the lack of discrimination by the promiscuous intermediate (Ab²) and determined the overall binding selectivity of SPE7 as seen in the final, high-affinity complexes.

Multispecificity mediated by conformational diversity. The second mode by which SPE7 exhibited multispecificity is through preexisting conformational diversity. This enabled SPE7 to bind antigens at either end of the structural spectrum, from small haptens to

a protein. The binding-site features of hapten-binding and protein-binding antibodies are quite different and are routinely seen in distinctly different antibodies (25). Here they were captured within a single antibody sequence. The Trx-Shear3:SPE7 structure (Ab⁴) had a long and flat binding site, whereas the hapten-bound structures (Ab³) had a deep and narrow pocket (Fig. 1). The binding site of SPE7 is also reminiscent of the binding site of an autoantibody: autoantigen, where the binding interactions occur on a surface almost perpendicular to the conventional antibody binding site (26). Part of the Trx-Shear3:SPE7 interaction involved a similarly placed surface that was not used in binding of the immunizing hapten.

This highlights the potential role that conformational diversity may have in triggering autoimmune syndromes and, by extension, allergy. The link between cross-reactive antibodies produced during infection and the subsequent development of autoimmunity is well known. Could an antibody bind a bacterial antigen with one preexisting isomer and a self-antigen with another? During infection, binding to the bacterial antigen would drive the equilibrium away from the self-binding isomer. Once the bacterial antigen was cleared, the antibody would be free to bind self-antigens. In allergy, cross-reactive IgE antibodies mediate uncontrolled mast-cell degranulation. Studies *in vitro* indicate that SPE7 is capable of initiating this process in the absence of the immunizing hapten (27, 28). Our results suggest that SPE7 could potentially mediate activation through promiscuous antigens that may be present in the media, which is consistent with the inhibition of SPE7-mediated mast-cell activation by DNP derivatives (28).

Conformational diversity in mature and germline antibodies. The effect of affinity maturation on antigen specificity and conformational diversity has seen considerable investigation. It has been proposed that germline antibodies complex antigen through one of many preexisting isomers and that during affinity maturation, mutations stabilizing the binding isomer are selected (17). The structures of several matured antibodies and their putative germline precursors have been determined. It was found that although the structures of free and complexed germline antibodies differ substantially, those of free and complexed mature antibodies are identical (15, 29). However, without solution kinetics, these differences cannot be unambiguously ascribed to preexisting conformational diversity. Furthermore, preexisting isomers and induced-fit conformational changes have been identified in many mature antibodies [for examples, see (11, 17, 30)], even when the structures suggest that the complexed and free antibody do not differ (31). Here we describe conformational diversity in a mature antibody. The work of Stevens, Schultz, and colleagues (15, 29) suggests that we should expect even greater diversity in germline antibodies.

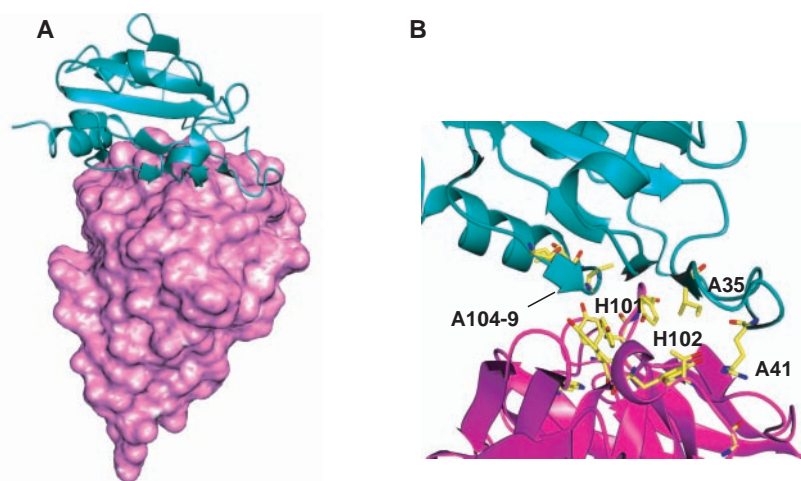


Fig. 5. Global topography and close-up of SPE7 Fv in complex with the protein ligand Trx-Shear3. (A) SPE7 is shown in surface representation (pink); Trx-Shear3 is shown in secondary structure representation (teal). (B) A close-up view of the SPE7 secondary structure is shown with side chains of the interacting residues. Trx-Shear3 is shown in teal; residues contacting SPE7, from both the Shear3 peptide loop (A35 to A41) and the thioredoxin scaffold (A104 to A109), are indicated.

Finally, in a wider context, our findings question the generally accepted notion of one sequence \rightarrow one structure \rightarrow one function. They are, however, in agreement with the view of proteins as an ensemble of preexisting isomers (32–34) that in some cases include intrinsically disordered proteins (35, 36). The latter often mediate specific binding to more than one ligand (34, 35), as is the case with SPE7. In both cases, so it seems, dissociation of unsuitable ligands is coupled to either global or local unfolding or to a major conformational change, whereas specific ligands induce a lock-in isomerization.

References and Notes

1. L. Pauling, *J. Am. Chem. Soc.* **62**, 2643 (1940).
2. K. Landsteiner, *Wein. Klin. Wochenschr.* **10**, 439 (1897).
3. P. Ehrlich, *J. Morgenroth, Berl. Klin. Wochenschr.* **38**, 569 (1901).
4. R. B. Christian, R. N. Zuckermann, J. M. Kerr, L. Wang, B. A. Malcolm, *J. Mol. Biol.* **227**, 711 (1992).
5. J. M. Varga, G. Kalchschmid, G. F. Klein, P. Fritsch, *Mol. Immunol.* **28**, 641 (1991).
6. A. Kramer *et al.*, *Cell* **91**, 799 (1997).
7. M. H. Kaplan, M. Meyesian, *Lancet* **1**, 706 (1962).
8. M. B. Oldstone, *FASEB J.* **12**, 1255 (1998).
9. S. Vieths, S. Scheurer, B. Ballmer-Weber, *Ann. N.Y. Acad. Sci.* **964**, 47 (2002).
10. M. L. Santiago *et al.*, *Int. Arch. Allergy Immunol.* **117**, 94 (1998).
11. J. H. Arevalo *et al.*, *J. Mol. Biol.* **241**, 663 (1994).
12. C. H. Trinh, S. D. Hemmington, M. E. Verhoeyen, S. E. Phillips, *Structure* **5**, 937 (1997).
13. B. A. Fields, F. A. Goldbaum, X. Ysern, R. J. Poljak, R. A. Mariuzza, *Nature* **374**, 739 (1995).
14. I. A. Wilson, R. L. Stanfield, *Curr. Opin. Struct. Biol.* **4**, 857 (1994).
15. F. E. Romesberg, B. Spiller, P. G. Schultz, R. C. Stevens, *Science* **279**, 1929 (1998).
16. D. Lancet, I. Pecht, *Proc. Natl. Acad. Sci. U.S.A.* **73**, 3549 (1976).
17. J. Foote, C. Milstein, *Proc. Natl. Acad. Sci. U.S.A.* **91**, 10370 (1994).
18. Z. Eshhar, M. Ofarim, T. Waks, *J. Immunol.* **124**, 775 (1980).
19. Materials and methods are available as supporting material on Science Online.
20. The sequence of SPE7 is most similar to IgG antibody B1-8 to NP (19) (fig. S1). The experiments were performed primarily with the recombinant Fv fragment of SPE7 Fv cloned from complementary DNA of the SPE7.49 hybridoma (18) and expressed in *Escherichia coli* [(19), section 1].
21. Pre-steady-state kinetics were performed and analyzed essentially as described (31); further details are given in section 2 of (19).
22. L. James, D. Tawfik, in preparation.
23. Z. Lu *et al.*, *Biotechnology* **13**, 366 (1995).
24. F. D. Batista, M. S. Neuberger, *Immunity* **8**, 751 (1998).
25. A. V. Collis, A. P. Brouwer, A. C. Martin, *J. Mol. Biol.* **325**, 337 (2003).
26. A. L. Corper *et al.*, *Nature Struct. Biol.* **4**, 374 (1997).
27. K. Asai *et al.*, *Immunity* **14**, 791 (2001).
28. J. Kalcsnikoff *et al.*, *Immunity* **14**, 801 (2001).
29. G. J. Wedemayer, P. A. Patten, L. H. Wang, P. G. Schultz, R. C. Stevens, *Science* **276**, 1665 (1997).
30. I. A. Wilson, R. A. Stanfield, *Curr. Opin. Struct. Biol.* **4**, 857 (1994).
31. A. B. Lindner, Z. Eshhar, D. S. Tawfik, *J. Mol. Biol.* **285**, 421 (1999).
32. B. F. Volkman, D. Lipson, D. E. Wemmer, D. Kern, *Science* **291**, 2429 (2001).
33. G. F. Joyce, *Science* **276**, 1658 (1997).
34. B. Ma, M. Shatsky, H. J. Wolfson, R. Nussinov, *Protein Sci.* **11**, 184 (2002).
35. P. E. Wright, H. J. Dyson, *J. Mol. Biol.* **293**, 321 (1999).

36. T. K. Hitchens, B. Mannervik, G. S. Rule, *Biochemistry* **40**, 11660 (2001).
37. Crystals were grown under the conditions described in Table 1. Details regarding crystal structure determination and additional data are given in section 3 of (19), including a Ramanchandran plot (fig. S2), electron density maps (fig. S3), B values (table S1), and a list of the interactions between SPE7 and the various ligands (table S2).
38. Collaborative Computational Project, No. 4, version 4.2, *Acta. Cryst.* **D50**, 760 (1994).
39. A. Nicholls, K. Sharp, B. Honig, *Proteins Struct. Funct. Genet.* **11**, 281 (1991).
40. A. Nicholls, B. Honig, *J. Comp. Chem.* **12**, 435 (1991).
41. Used with kind permission of M. E. M. Noble, unpublished.
42. S. V. Evans, *J. Mol. Graph.* **11**, 134 (1993).
43. Single-letter abbreviations for the amino acid residues are as follows: A, Ala; C, Cys; D, Asp; E, Glu; F, Phe; G,

- Gly; H, His; I, Ile; K, Lys; L, Leu; M, Met; N, Asn; P, Pro; Q, Gln; R, Arg; S, Ser; T, Thr; V, Val; W, Trp; and Y, Tyr.
44. This article is dedicated to the beloved memory of Cesar Milstein. We are grateful to T. Waks, Z. Eshhar, and A. Bloomer for their support; to P. Evans, G. Evans, A. Leslie, E. Blanc, and G. Bricogne for help and advice with data collection and structure determination; and to I. Wilson for constructive criticism. Supported by a Wellcome Trust grant.

Supporting Online Material

www.sciencemag.org/cgi/content/full/299/5611/1362/DC1
Materials and Methods
Figs. S1 to S6
Tables S1 and S2
References and Notes

24 October 2002; accepted 17 January 2003

Spectroscopic Determination of the OH⁻ Solvation Shell in the OH⁻·(H₂O)_n Clusters

William H. Robertson, Eric G. Diken, Erica A. Price, Joong-Won Shin, Mark A. Johnson*

There has been long-standing uncertainty about the number of water molecules in the primary coordination environment of the OH⁻ and F⁻ ions in aqueous chemistry. We report the vibrational spectra of the OH⁻·(H₂O)_n and F⁻·(H₂O)_n clusters and interpret the pattern of OH stretching fundamentals with ab initio calculations. The spectra of the cold complexes are obtained by first attaching weakly bound argon atoms to the clusters and then monitoring the photoinduced evaporation of these atoms when an infrared laser is tuned to a vibrational resonance. The small clusters ($n \leq 3$) display an isolated, sharp feature near the free OH stretching vibration, the signature of open solvation morphologies where each water molecule binds independently to the ion. Pronounced changes in the spectra are observed at $n = 4$ in the hydroxide ion and at $n = 5$ in the fluoride ion. In both cases, new features appear in the region typically associated with interwater hydrogen bonding. This behavior establishes that the primary hydration shells occur at $n = 3$ and 4 in hydroxide and fluoride, respectively.

The hydroxide ion (OH⁻) is one of the two essential ionic species in aqueous chemistry (1), but its microscopic, molecular-level character, when associated with water, is still actively discussed (2–5). The major difficulty introduced by OH⁻ arises from its very high proton affinity, which causes the ionic H-bond to explore the symmetrical [HO··H··OH]⁻ Zundel-type structures. Indeed, such shared proton motifs lie at the heart of the anomalous mobility displayed by OH⁻ in water (6).

Most simulations indicate that three or four water molecules are in direct contact with OH⁻ in aqueous solution, and Parrinello (3, 7), for example, has concluded that population of the higher energy tetrahedral (trihydrate) form is the key to proton transport. We present vibrational spectra of the cold OH⁻·(H₂O)_{1–5} cluster ions

that display sharp, well-defined bands in the OH stretching region. These spectra are then analyzed with the aid of ab initio calculations to identify the structural motifs at play in the size regime of the putative shell closing. To clarify the distinctive aspects of OH⁻ hydration, we contrast its behavior with similar spectra obtained for cold F⁻·(H₂O)_n clusters in the same size range. This system was chosen because the F⁻ hydrates are predicted (8, 9) to adopt morphologies similar to those anticipated to occur in the OH⁻ hydrates.

Previous studies and experimental design. In previous work on these systems, thermochemical measurements (10) of the sequential water binding energies for the OH⁻·(H₂O)_n clusters indicate a break at $n = 4$, although similar measurements on the fluoride hydrates do not suggest a shell closing (10, 11). The break in the OH⁻ hydrates was interpreted to reflect a shell closing at $n = 3$, but this hypothesis is somewhat tempered by the lack of discontinuities in the binding energies in OD⁻·(D₂O)_n analogs (12). Theoretical work

Sterling Chemistry Laboratory, Department of Chemistry, Yale University, Post Office Box 208107, New Haven, CT 06520–8107, USA.

*To whom correspondence should be addressed.
E-mail: mark.johnson@yale.edu